Journal Name

ARTICLE TYPE

Cite this: DOI: 10.1039/xxxxxxxxxx

Electric Birefringence Spectroscopy of Montmorillonite Particles

Paloma Arenas-Guerrero,[a] Guillermo R. Iglesias,[a] Ángel V. Delgado[a] and María L. Jiménez*[a]

Received Date
Accepted Date

DOI: 10.1039/xxxxxxxxxx

www.rsc.org/journalname

Electric birefringence (EB) of suspensions of anisotropic particles can be considered an electrokinetic phenomenon in a wide sense, as both liquid motions and polarization of the electrical double layer (EDL) of the particles participate in the process of particle orientation under the applied field. The EB spectrum can be exploited for obtaining information on the dimensions, average value and anisotropy of the surface conductivity of the particles, and concentration and Maxwell-Wagner polarization of the EDLs. It is thus a highly informative technique, applicable to non-spherical particles. In this paper, we investigate the birefringent response of plate-like montmorillonite particles as a function of the frequency and amplitude of the applied AC electric field, for different compositions (pH, ionic strength, particle concentration) of the suspensions. The transient electric birefringence (i.e., the decay of the refractive index anisotropy with time when the field is switched off) is used for estimating the average dimensions of the particle axes, by modeling it as an oblate spheroid. The obtained values are very similar to those deduced from electron microscopy determinations. The frequency spectra show a very distinct behaviour at low (on the order of a few Hz) and high (up to several MHz) frequencies: the α and Maxwell-Wagner-O'Konski relaxations, characteristic of EDLs, are detected at frequencies above 10 kHz, and they can be well explained using electrokinetic models for the polarization of EDLs. At low frequencies, in contrast, the birefringence changes to negative, an anomalous response meaning that the particles tend to orient with their symmetry axis parallel to the field. This anomaly is weaker at basic pHs, high ionic strengths and low concentrations. The results can be explained by considering the polydispersity of real samples: the fastest particles redistribute around the slowest ones, inducing a hydrodynamic torque opposite to that of the field, in close similarity with results previously described for mixtures of anisometric particles with small amounts of spherical nanoparticles.

1 Introduction

The optical properties of suspensions of non-spherical colloidal particles can be modified by the application of an electric field.[1–3] One of these electro-optical effects is the electric birefringence (EB), that is, the anisotropy of the refractive index of the suspension caused by the electrically induced orientation of the particles. The analysis of EB has been proposed as a suitable technique for the characterization of non-spherical particles,[1–6] as it is susceptible to provide much useful information not only about the optical, electrical and geometrical properties of the particles in suspension, but also about the electrokinetic phenomena taking place at their interfaces. For instance, Transient Electric Birefringence (TEB), the study of the dynamic response of the system, is utilized to examine the size distribution of the particles in the sample,[2,7–10]. Electric Birefringence Spectroscopy (EBS), the analysis of the behaviour of the birefringence as a function of the frequency of the applied field, albeit yet incomplete, can provide exhaustive information about the different polarization mechanisms of the nanoparticles and their electric double layers (EDLs).[2,5,6,10–13]

However, although the foundations of the electric birefringence have been long-established, the process is hitherto not understood on the whole and cannot yet be considered as a widespread characterization technique.[12,14–16] Thus, microscopic models relating the nanoparticle properties to their macroscopic birefringent response are to date not completely satisfactory.[6,8,12,13] For instance, only simplified geometries are considered; the effect of the polydispersity of the sample and the presence of interparticle interactions are taken into account partially if at all; the effect of the hydrodynamic torque is normally neglected[13] and the contribution of a heterogeneous charge distribution is still an open

[a] Department of Applied Physics, School of Science, University of Granada, 18071 - Granada, Spain. E-mail: jimenezo@ugr.es

question.[13,17,18] Consequently, further research of the topic is needed, not only from an applied point of view, but also at a fundamental level.

Similar to other laminar materials, sodium montmorillonite (NaMt) is a good candidate for the analysis of EB, since these clay particles are known to possess a non-homogeneous and pH-dependent charge.[19–22] Moreover, it has been found that suspensions of sodium montmorillonite and similar clays exhibit a negative (anomalous) birefringence,[14,23,24] sparking interest in the phenomenon. The mentioned anomaly consists in the tendency of the particles to orient under some conditions with their major axis perpendicular to the external field, instead of parallel, as in "normal" EB. In dilute suspensions, negative birefringence has been recently reported for a variety of materials,[10,15,16,25,26] and in most cases it cannot be explained theoretically inside a classical framework.

With this motivation, in this article we will focus our attention on the study of the birefringence phenomenology of sodium montmorillonite suspensions. Firstly, TEB experiments are performed together with electron microscopy determinations in order to estimate the size distribution of the sample. Thereupon, an extensive examination of the spectral response of this material is carried out in order to study the electrical properties of the particles and the origin of the anomalous response.

2 Theory

2.1 Electro-orientation of non-spherical particles.

When an electric field E is applied to a colloidal suspension, an electric dipole is induced on the particles.[27–29] If these are not spherical, their electric polarizability is anisotropic,[5,11,13,30] and for axially symmetric particles, this anisotropy can be expressed by the scalar quantity $\Delta\alpha^e = \alpha_b^e - \alpha_a^e$, being $\alpha_b^e(\alpha_a^e)$ the electric polarizability along their major(minor) axis, b and a, respectively. In general, this quantity is different from zero, and hence, the total dipole moment induced by an applied field is not parallel to the latter. As a consequence, it appears an electric torque that tends to orient the particle with its major axis parallel to the external field.

In addition, most non-spherical nanoparticles exhibit anisotropic optical polarizability $\Delta\alpha^o = \alpha_b^o - \alpha_a^o$, due to their shape and/or their anisotropic crystal structure. Normally, when the particles are suspended in an electrolyte solution, their orientation is random and the system is optically isotropic on a macroscopic scale. However, upon application of an external electric field, particles orient, giving rise to an anisotropy in the refractive index of the suspension known as birefringence and given by[1]

$$\Delta n = \frac{\Delta\alpha^o \phi \langle P_2(\cos\theta)\rangle}{2 n_s \varepsilon_0 V_p} \tag{1}$$

where ϕ is the volume fraction of dispersed particles, n_s the refractive index of the suspending solution, ε_0 the vacuum permittivity and V_p the particle volume. $\langle P_2(\cos\theta)\rangle$ is the average value of the second Legendre polynomial of the orientational distribution, which is a measure of the degree of alignment of the particles with the external electric field.

In this contribution we restrict ourselves to diluted suspensions of particles with no intrinsic dipole moment and we work in the low field range, where expansions in power series of E are usable. In these conditions, and neglecting the viscous forces (which is a good approximation for high frequency fields[12]) an explicit expression of Δn is available[5]

$$\Delta n = \frac{\Delta\alpha^o \Delta\alpha^e \phi E_0^2}{30 n_s k_B T V_p} \tag{2}$$

Here k_B is the Boltzmann constant, T the temperature and E_0 the field amplitude. The quadratic dependence of the birefringence on E_0 is known as Kerr's law and allows us to define the Kerr constant, a magnitude independent of the field strength, as

$$K = \frac{\Delta n}{\lambda E_0^2} \tag{3}$$

where λ is the wavelength of the incident light beam.

2.2 Transient Electric Birefringence (TEB).

Upon removal of the external electric field, rotational diffusion due to thermal agitation will randomize the orientation of the nanoparticles in a finite time. The subsequent decay of the birefringence is expected to be in the form of a simple exponential for monodisperse samples; for the more realistic case of polydisperse samples, however, the relaxation of the birefringence must be computed as a superposition of independent exponential processes. In this manner, under reasonable assumptions, it can be shown that $\Delta n(t)$ presents the shape of a stretched exponential function[8]

$$\Delta n(t) = \Delta n_0 \exp\left[-(t/\tau)^\alpha\right] \tag{4}$$

where τ is a characteristic decay time and α a polydispersity factor. These two parameters provide an average rotational diffusion coefficient Θ for the particles in suspension by the relation[8]

$$\Theta = \frac{\alpha}{6\tau\Gamma(1/\alpha)} \tag{5}$$

where Γ is the Euler gamma function.

This coefficient depends on the third power of the particle size, and therefore its measurement can provide a good estimation of the size distribution of the sample. The diffusion coefficient is related solely to the particle's size and shape, and analytical expressions are available for simple geometries. In this work we have modeled our particles as oblate ellipsoids of major axis b and aspect ratio $\rho = b/a$. In this case, Θ can be written as[31]

$$\Theta = \frac{3k_B T}{16\pi\eta a^3}\left[\frac{(2-\rho^2)(1-\rho^2)^{-1/2}\arctan(\sqrt{\rho^2-1}) - 1}{1-\rho^4}\right] \tag{6}$$

being η the viscosity of the suspending medium. Making use of eqns (5) and (6), an estimation of the average particle size can be calculated from TEB measurements.

2.3 Electric Birefringence Spectroscopy (EBS).

When the electric field applied to the suspension is alternating, Δn can be separated into two spectral components: a time-independent DC component or steady-state birefringence and an AC component oscillating with twice the frequency ν of the field

$$\Delta n = \Delta n_{DC}(\nu) + \Delta n_{AC}(\nu)\sin(4\pi\nu t) \quad (7)$$

The spectral behaviour of Δn_{DC} and of Δn_{AC} furnish information about different properties of the particles in the suspension. On the one hand, the amplitude of the AC oscillations decreases with ν, becoming negligible at a certain value of the frequency of the applied field. Such value gives an idea of the characteristic time at which the particles can no longer follow the field oscillations, and therefore provides an estimation of the particle size.

On the other hand, the spectral behaviour of the DC term is related to the relaxations of the particle's dipole, and hence a thorough analysis of the Δn_{DC} spectrum is very useful for the characterization of the electrical properties of the nanoparticles in suspension. Because the AC component averages to zero over time, the DC Kerr constant can be defined as

$$K(\nu) = \frac{2\langle \Delta n(\nu)\rangle}{\lambda E_0^2} \quad (8)$$

Normally, two relaxations can be observed in the DC birefringence spectrum of colloidal suspensions, namely, the α and the Maxwell-Wagner-O'Konski (MWO) relaxations. The α relaxation is related to the concentration polarization, which is in turn produced by the different transport numbers of coions and counterions in the double layer.[28] The characteristic frequency for the α relaxation can be estimated as $\nu_\alpha \sim D/R^2$, being D the diffusion coefficient of the ions in solution and R the characteristic diffusion length, of the order of the particle size. If the frequency of the field is larger than ν_α the concentration polarization mechanism cannot be established and therefore can no longer contribute to the formation of the electric dipole. In this case, the dipole is determined by the MWO polarization mechanism. For spherical and insulating particles, it has been demonstrated[27] that MWO electric polarizability is the same as that of a conductive particle with an effective conductivity of $K^{eff} = 2K^\sigma/R$, being K^σ the surface conductivity. This is normally the case of colloidal particles, where the excess of conduction in the EDL can be simulated as a surface conductivity. If particles are not spherical, the effective conductivity is different for the two axes, $K_{b,a}$,[13] being the relation between them a geometrical factor in the case of homogeneous charge. For the case of non-homogeneously charged particles this relation is not geometrically determined.[2] This polarization relaxes at a characteristic frequency, ν_{MWO}, determined by the particle and medium conductivities and permittivities.[27] When $\nu > \nu_{MWO}$, the free charges in the EDL of the particle cannot successfully redistribute anymore and only the molecular polarization contributes to the dipole formation.

3 Materials and Methods

3.1 Materials

NaMt was obtained from bentonite (Serrata de Níjar, Spain) by a process of homoionization[20] consisting in successive rinses of the clay with a 1 M sodium chloride solution; surplus ions were removed by repeated cycles of centrifugation and redispersion in deionized water (Milli-Q Academic, Millipore, France). The resulting NaMt gel was dried and put aside for sample preparation.

Sodium montmorillonite is a laminar clay with negative charge on the faces and a pH dependent charge on the edges,[19,20] whose isoelectric point is located at pH 7, a value close to the natural pH of the NaMt suspensions (6.8). The average dimensions of the particles were firstly determined by environmental scanning electron microscopy (ESEM, FEI Quanta 250 SEM, The Netherlands). This technique allows us to maintain a certain level of humidity (around 20 % in our case) in the chamber, avoiding particle aggregation. As a result, individual particles can be distinguished, as shown in Fig. 1a. From this image, the histogram in Fig. 1b is obtained and the average length (by volume) of the major axis of the particles is estimated as 1.7 ± 0.6 μm. In addition, in Fig. 1a we can see that the particles are planar, and hence, we can approximate their shape by oblate spheroids.

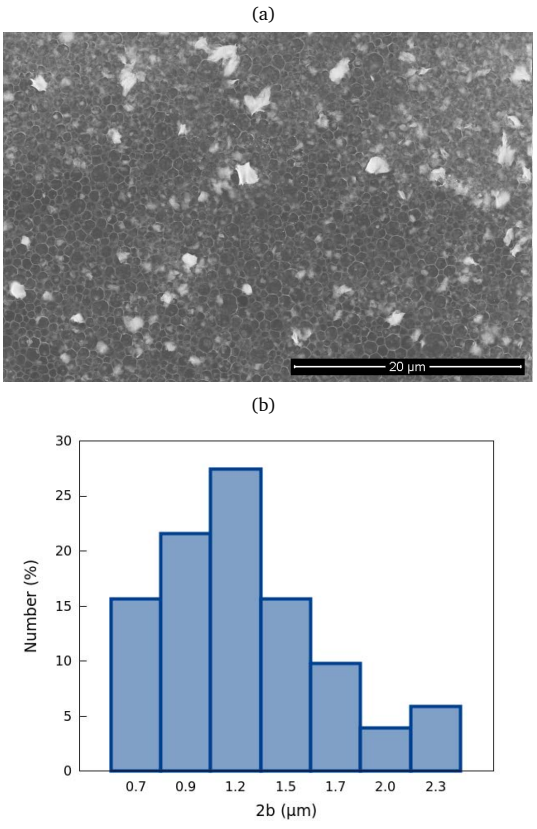

Fig. 1 Geometrical characterization of the clay particles. a) ESEM picture of a NaMt sample; b) histogram of the largest axis lengths obtained from a).

3.2 Methods

The electric birefringence of the suspensions is obtained via the analysis of the polarization of light after passing through the samples.[4,32] In the experimental setup, a He-Ne laser beam traverses *i)* a polarizer at 45° to the electric field, *ii)* the suspension, *iii)* a quarter-wave plate whose fast axis is placed parallel to the polarizer axis and *iv)* an analyser at $90^\circ - \alpha$ to the initial polarization. All the optical elements were purchased from Edmund Optics, UK.

The sample is placed in an optically neutral quartz cell of 1 cm path length (Starna Scientific, UK), thermostated at $15.0 \pm 0.2^\circ$C, and subjected to an external uniform electric field via vertical planar stainless steel electrodes immersed in it and separated 1 mm. Sinusoidal electric field pulses (duration of 5 s) in a frequency range of 1 Hz-10 MHz are sent to the electrodes from a commercial generator (Tektronix AFG 3101, USA). The light intensity transmitted through the optical setup is collected by a photodiode (Edmund Optics T59-142, UK) connected to a digital oscilloscope (Tektronix TDS 2012C, USA). The data acquisition and analysis are computer controlled. The light intensity I reaching the photodiode at time t is directly related to the birefringence of the sample, $\Delta n(t)$, by[33]

$$\Delta n(t) = \frac{\lambda}{\pi l}\left[\arcsin\left(\sqrt{\frac{I(t)}{I_0}}\sin\alpha\right) - \alpha\right] \qquad (9)$$

where I_0 is the intensity transmitted by the setup when no electric field is applied and l is the path length. In order to determine the steady-state birefringence, the plateau region of 1 or 2 pulses is averaged over time. The stress birefringence introduced by the cell is subtracted as indicated elsewhere.[33]

4 Results and Discussion

4.1 General features

In Fig. 2 the birefringent response of a sample of NaMt subjected to electric field pulses is shown. As observed, the shape of the transient behavior of the DC component is independent of the frequency of the applied field. Systematic measurements do not show any dependence on the particle concentration, ionic strength, pH of the sample, field strength, and pulse duration. On the other hand, the AC oscillations can only be observed for the 1 Hz data, being negligible for other presented frequencies. This can be seen in a more detailed way in Fig. 3a, where the amplitude of the AC oscillations as a function of the frequency of the applied field is presented. The oscillations decay strongly with ν, becoming negligible at a frequency of about 100 Hz. This behavior indicates that for times shorter than 0.01 s the particles are not able to follow the field oscillations, which is expected for micron-sized particles.

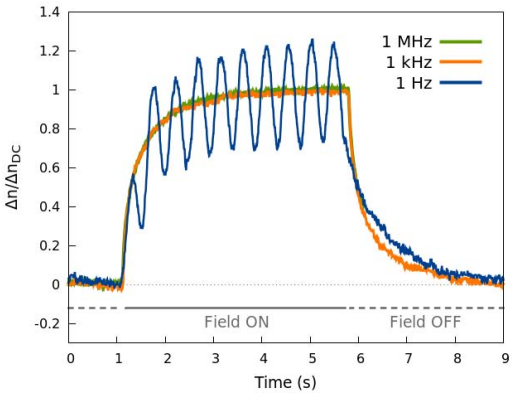

Fig. 2 Birefringent response (relative to the stationary DC value) of a sample of NaMt 1 g/L and 0.3 mM NaCl when subjected to field pulses of different frequencies, 5 seconds of duration and a field amplitude of 10 V/mm.

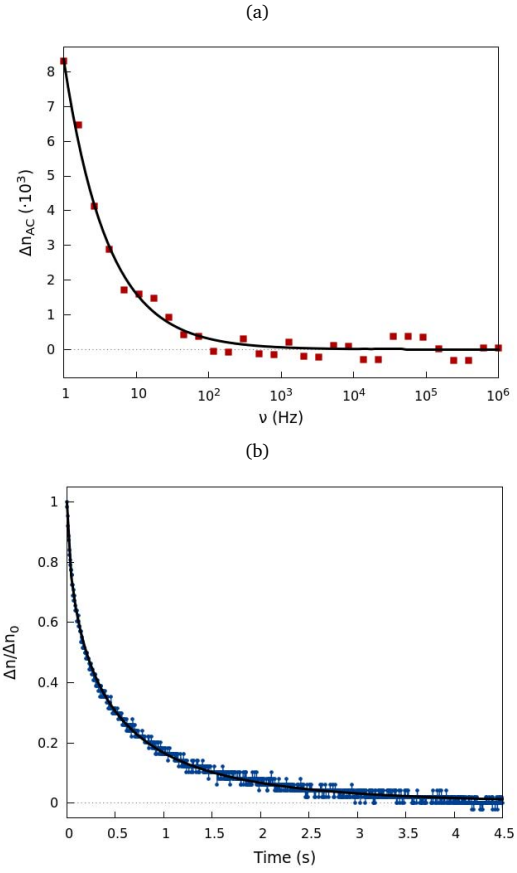

Fig. 3 EB measurements of a sample of NaMt 1 g/L and 0.3 mM NaCl; the field amplitude is 10 V/mm. a) Spectrum of the AC component of the birefringence. The line is a guide to the eye. b) Birefringent response (relative to the stationary DC value) of the sample when subjected to field pulses of different frequencies and 5 seconds of duration.

A more precise estimation of the particle size can be achieved from TEB measurements. In Fig. 3b, the obtained decay of the birefringence after the field is turned off is presented together with a fit of the data via a stretched exponential function (eq 4). From the obtained values of τ and α (374 ± 2 ms and 0.593 ± 0.002,

respectively), making use of eqns (5) and (6), and assuming $\rho = 3$, we obtain a diameter of 1.9 μm for these particles. This value is very similar to the one obtained via ESEM pictures, differing from it by no more than 20%, a deviation comparable to that found for other planar particles.[10] These results show that, even though our sample is polydisperse, this method is adequate for the estimation of the particle size.

In our experiments, Kerr's law is satisfied in all case for $E_0 < 11$ V/mm. At larger fields, deviation from this law due to saturation of the birefringence is observed, in agreement with the data reported elsewhere[22] where it was found that linearity with E_0^2 is lost above 20 V/mm for similar clays. Hereafter all experiments are performed with an electric field of 10 V/mm and hence, the Kerr constant can be properly used.

Fig. 4a shows a typical birefringence spectrum of NaMt. It exhibits a complex structure with different dispersion processes. As already pointed, if only the electric torque promoted by the external field is taken into account, the Kerr constant is proportional to the polarizability anisotropy (see eq 2), and hence, the dispersion in Fig. 4a is a manifestation of the different electrokinetic processes that contribute to the induced polarization. The theoretical expectations are depicted in Fig. 4b for oblate spheroids with a radius of 800 nm and an aspect ratio of 3, suspended in 0.3 mM NaCl solution. In these and subsequent calculations, the models used are those in Refs.[5,13]. Note that, since the polarizability anisotropy is a balance between the polarizabilities along the main axes, a rise in α_b (α_a) yields to an increase (decrease) in $\Delta\alpha_e$. A decrease is expected in the polarizabilities in the MHz range, due to the freezing of the MWO polarization mechanism. The MWO dipole is promoted by the mismatch between particle/EDL and medium conductivities and usually takes the same direction of the applied field, that is, it produces a positive polarizability. In the kHz range, in turn, the concentration polarization beyond the EDL will undergo a strong reduction. Recall that this phenomenon produces a deformation of the double layer and separation of the centres of the particles and its EDL cloud, which gives rise to a negative contribution to the polarizability. Because of this, the α relaxation brings about an increase of $\alpha_{a,b}$.

For homogeneous particles (dashed line in Fig. 4b), the polarizability along the long axis is usually larger, and hence, $\Delta\alpha_e > 0$. Furthermore, the characteristic frequency of the α relaxation is mainly dependent on the particle geometry, and is similar for α_a^e and α_b^e: from this, the α relaxation manifests as an increase in $\Delta\alpha_e$. On the other hand, the characteristic frequency of MWO is highly dependent on the conductivity, being smaller for the longer semiaxis b. This means that in the MWO frequency range, α_b^e relaxes at lower frequency, which manifests in a dip in $\Delta\alpha_e$. However, the most relevant results is the contrast with the case of non-homogenous charge distribution (solid lines in Fig. 4b). In this case, there is a decrease in K_a. For this reason, in the MHz range α_a^e relaxes at a lower frequency than α_b^e, and the MWO relaxation appears as a hump in $\Delta\alpha_e$.

The features of the electrokinetic predictions in Fig. 4b are in line with the experimental results of Fig. 4a. In the kHz range there exists an increase of the Kerr constant which corresponds to the α relaxation. This increase occurs at a frequency compara-

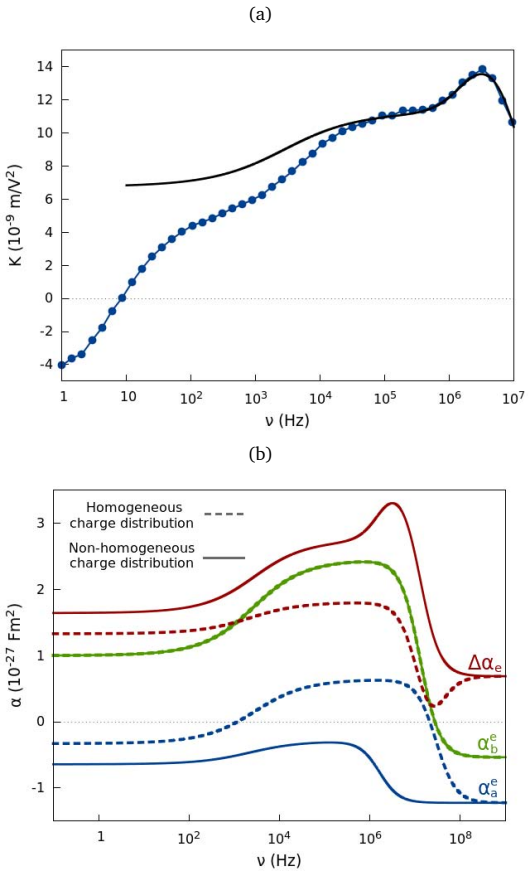

Fig. 4 a) Kerr constant of NaMt suspensions (1 g/L particles, 0.3 mM NaCl) as a function of the frequency of the applied field. The points are the experimental data and the line is the electrokinetic prediction. Field strength 10 V/mm. b) Theoretical predictions for the electric polarizability along the major (α_b^e) and minor (α_a^e) axes of the particles and for its anisotropy ($\Delta\alpha^e$). Two cases are analysed: homogeneous ($K_a/K_b = 0.27$) and heterogeneous ($K_a/K_b = 0.008$) charge distribution. The particles are oblate spheroids with major semiaxis $b = 800$, aspect ratio $b/a = 3$ and $K_b = 0.25$ S/m. Dispersion medium: 0.3 mM NaCl.

ble to that expected from electrokinetic calculations, although the amplitude of the jump is larger than predicted. This can be understood, since in the kHz range the hydrodynamic torque, not taken into account in the theoretical calculations, can play an important role on the orientation of the particles.[12] In the MHz range, the hump and final decay in the spectrum is well reproduced by the electrokinetic model. In the Hz range the birefringence presents a negative value that is not predicted by classical electrokinetics, and as found by other authors working with sodium montmorillonite and similar clays.[14,16,23,24,26] Note that the negative values correspond to an anomalous orientation of the particle, with its axis of symmetry along the electric field. The characteristic frequency of this process (ν_c) is located at around 7 Hz.

Some features of the spectrum are similar to those presented by other planar particles like gibbsite in Ref.[10], although the Kerr constant values and the MWO relaxation frequency are much higher in the present work because of the larger particle size and surface conductivity. For example, at 1 MHz, the value of the electrical polarizability is $\alpha_a^e = -5.49 \times 10^{-28}$ Fm^2 along the

symmetry axis and $\alpha_b^e = 2.41 \times 10^{-27}$ Fm^2 along the particle surface. In this case, the polarizability anisotropy per unit volume, $\Delta\alpha^e/V_p = 3.7 \times 10^{-9}$ F/m, is comparable to values obtained elsewhere[14,22] for similar materials.

From the experimental birefringence spectrum much information about the properties of the particles in suspension can be obtained. First, we determined the value of their optical anisotropy, $\Delta\alpha^o = 4.3 \times 10^{-33}$ Fm^2. This value corresponds to particles with a lower refractive index than the one of NaMt ($n = 1.5$) due to the swelling of this material:[19] sodium montmorillonite particles absorb water, which lowers their refractive index, thus reducing the magnitude of the Kerr constant. From the value of $\Delta\alpha^o$ we can calculate the refractive index of the swollen particles, and hence estimate their water content. The obtained value of the volume fraction, 88% of water, is in agreement with that found elsewhere[19,34] (90-93%) for the osmotic swelling of sodium montmorillonite.

From the electrokinetic predictions we can also obtain information about the geometrical properties of the particles in suspension. Note that the degree of swelling does not only affect the refractive index but also the aspect ratio of the hydrated particles, in the same proportion. In fact, from the experimental results we obtain an aspect ratio $\rho = 3.3$ for the swollen particles. Given the water content, this corresponds to an aspect ratio of 30 for the dry particles, a reasonable value for these particles. The obtained value of the major axis length is 1.6 μm, in good agreement with the average size obtained from both ESEM and TEB determinations.

4.2 Effects of pH and ionic strength

The birefringent response of sodium montmorillonite is modified substantially when the pH of the sample is changed, as can be clearly observed in Fig. 5a. This is an intriguing result, since the pH alters only the edge charge, which is much smaller than the surface charge. Note that these results cannot be caused by structure formation, since TEB experiments confirm that the transient behaviour is not altered by edge charge variation. Therefore it can be suggested that indeed the charge distribution plays an important role on particle electro-orientation.

The effect of the pH on the birefringence spectrum can be introduced in the electrokinetic predictions via the modification of the conductivity along the particle symmetry axis. The agreement between the experimental data and the theoretical predictions is very good for frequencies above 10^4 Hz (Fig. 5b), where the MWO dispersion is the predominant contribution. As it can be seen in Table 1, the pH modifies the particle's conductivity anisotropy, the more so at more acid pH, when the edges are charged positively in contrast with the negatively charged faces. However the experimental values are always far from the case of homogeneously charged particles, for which K_a/K_b=0.27.

The conductivity values K^σ are rather large, probably a manifestation of the presence of the Stern layer conductivity.[29,35,36] The latter comes from the motion of ions (not liquid) in the stagnant layer, that is, the volume comprised between the solid boundary of the particle and its slip or electrokinetic plane, which roughly corresponds to the beginning of the diffuse part of the EDL. The values presented agree with the estimations of K^σ obtained using DC conductivity[37] and dielectric spectroscopy[38] data, reported elsewhere for montmorillonite particles of the same origin as those used in this work. These authors found $K^\sigma = 4-6 \times 10^{-8}$ S, values comparable to our present data. Concerning the values of effective particle conductivity K^{eff}, our results ($K^{eff} = 0.05$ S/m) are almost identical to those reported in Ref.[37], as expected from the similarities between the samples.

The values of surface conductivity shown in Table 1 are however larger than those reported by other authors in layered materials. For instance, values found for the surface conductivity of kaolinite particles are in the order of $K^\sigma = 0.2 \times 10^{-8}$ S.[39,40] Another example can be found in Ref.[41], where a mixture of kaolinite, illite and smectite was analysed and a surface conductivity of $K^\sigma = 0.25 \times 10^{-8}$ S was reported. In addition, Dozov et al.[22] calculated $K^\sigma = 0.5 \times 10^{-8}$ S for beilledite particles. This corresponds to a larger value for K^{eff} (15 S/m in the latter case), that is, to highly conductive particles.

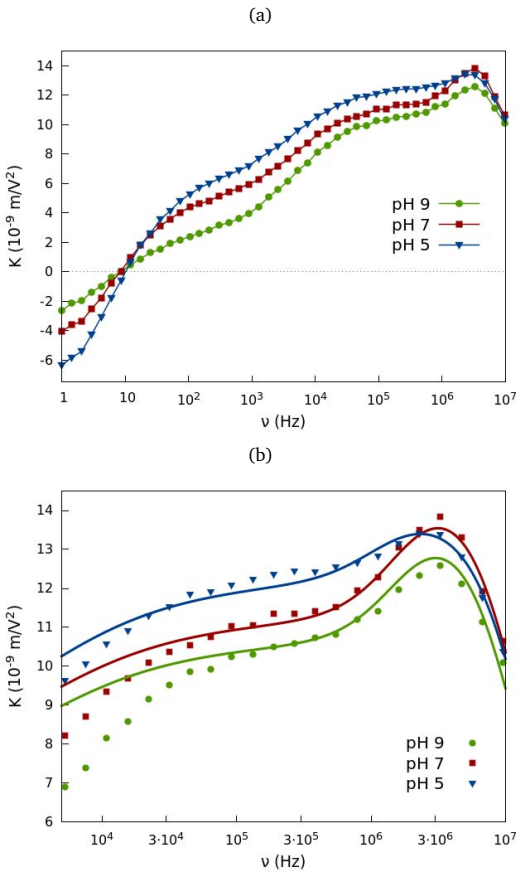

Fig. 5 Kerr constant spectra of NaMt suspensions (1 g/L and 0.3 mM NaCl) for the indicated pH values. a) Complete frequency range; b) detail of the high frequency region. The points are the experimental data and the lines in b) correspond to the predictions of the electrokinetic model.[13]

In Fig. 6 the EB spectra for different values of the ionic strength are shown. The same features as in the previous figures are observed, and a similar analysis provides the surface conductivities

Table 1 Values of the surface conductivity and charge anisotropy obtained from the fit of the electrokinetic expressions to the experimental data. The pH dependence is analysed at 0.3 mM NaCl. The ionic strength dependence is studied at pH 7

pH	K^σ (10^{-8} S)	K_a/K_b
5	4.4	0.003
7	4.0	0.008
9	3.7	0.009
NaCl (mM)	K^σ (10^{-8} S)	K_a/K_b
0.1	4.1	0.008
0.3	4.0	0.008
0.6	3.9	0.008
1	3.5	0.008

shown in Table 1. The relation K_a/K_b does not change appreciably, which is coherent with the fact that neither the edge nor the face charges are modified by changes in the ionic strength.

4.3 Low-frequency anomalous birefringence

As mentioned, it is remarkable that in the low frequency range there exists a reversal of the birefringence for all values of the pH and the ionic strength (Figs. 5a and 6a). Such an effect has been previously reported for a number of materials,[10,14–16,23–26] always for DC or slowly oscillating fields, and cannot be explained by classical electrokinetic theories.

The features of the anomalous effect for sodium montmorillonite samples can be summarized as follows. First, in Fig. 2 we observe that the dynamic behaviour is the same in the negative and positive birefringence regions, Kerr's law being always fulfilled. The negative effect is larger for more acid values of the pH (Fig. 5a), when the edge and face charges exhibit opposite sign. Regarding the ionic strength dependence, in Fig. 6a it can be seen that the anomalous birefringence is more pronounced for smaller values of the salt concentration.

A first hypothesis for the explanation of the negative effect could be the formation of structures. This can be ruled out since such phenomenon would lead to a change in the dynamic behaviour in the low frequency range, which is not detected. However, long range particle interactions are still plausible. In order explore this possibility, we studied the EB spectrum as a function of particle concentration C. The results are shown in Fig. 7a, where it can be observed that in the kHz and MHz ranges all curves collapse to the same values, indicating that the Kerr constant is proportional to the particle concentration. We can thus consider that the system is dilute and particle interactions can be neglected in the high frequency range. On the other hand, in the Hz range K/C depends strongly on the particle concentration. These results lead to the conclusion that the negative torque is caused by long-range particle interactions and rule out an explanation based on a single particle phenomenon. In Fig. 7b, the spectrum of the logarithmic derivative of the normalized Kerr constant ($\frac{1}{C}\frac{dK}{d\log\nu}$) is presented. Here, it can be observed that the shape of the curve is independent of the particle concentration. Thus, even though a larger value of the concentration yields a more pronounced negative effect, the characteristic frequency of the process does not depend on the volume fraction.

The negative birefringence can have either an electric or hydrodynamic origin. In the former approach, the existence of a permanent[23,24] or saturable induced[14,25] dipole moment for these particles has been proposed as possible explanation for this effect. However, a theory based only on the existence of a dipole of electric origin perpendicular to the particle surface cannot account for the concentration dependence found in Fig. 7a. Moreover, the fulfillment of Kerr's law is not compatible with the existence of a saturable induced dipole moment.

In order to explain this concentration dependence, a particle-concentration induced mechanism that gives rise to an overall perpendicular dipole moment was proposed in[16] to account for the anomalous orientation of laponite and hectorite. There it was argued that, for high concentrations, the overlapping of the EDLs of the edges of adjacent particles diminishes the polarization along the particle surface, leaving unperturbed the perpendicular component. At some point, the latter can reach larger values, leading to a preferred perpendicular orientation. Nevertheless, if this is the case, the effect should occur whatever the frequency of the applied field, in contrast to our results. In fact, since the Kerr constant does not depend on the particle concentration in the MHz, EDL overlapping can be ruled out as an explanation for our system. In addition, since the EDL is very thin in our case

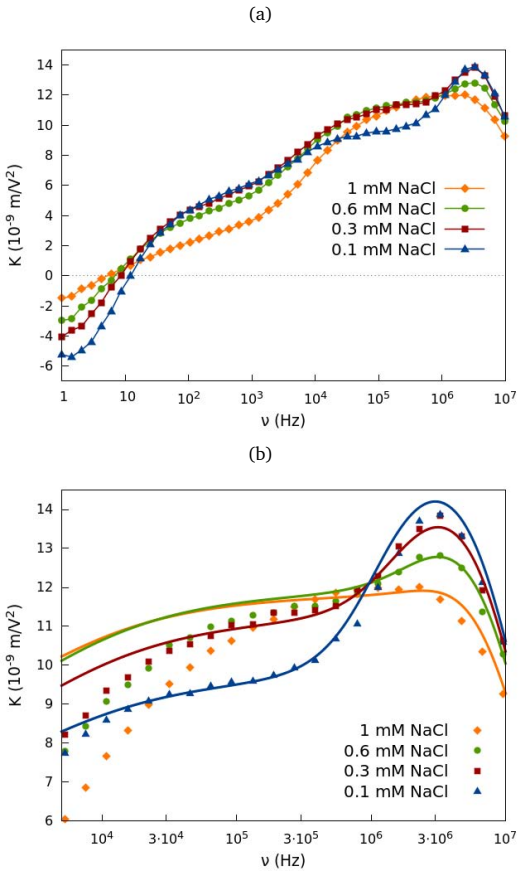

Fig. 6 EB spectra of samples of sodium montmorillonite (1 g/L, pH 7) with different values of the ionic strength: a) Complete frequency range, b) zoom in the high frequency range. The points are the experimental data and the lines in b) correspond to the predictions of the electrokinetic model.[13]

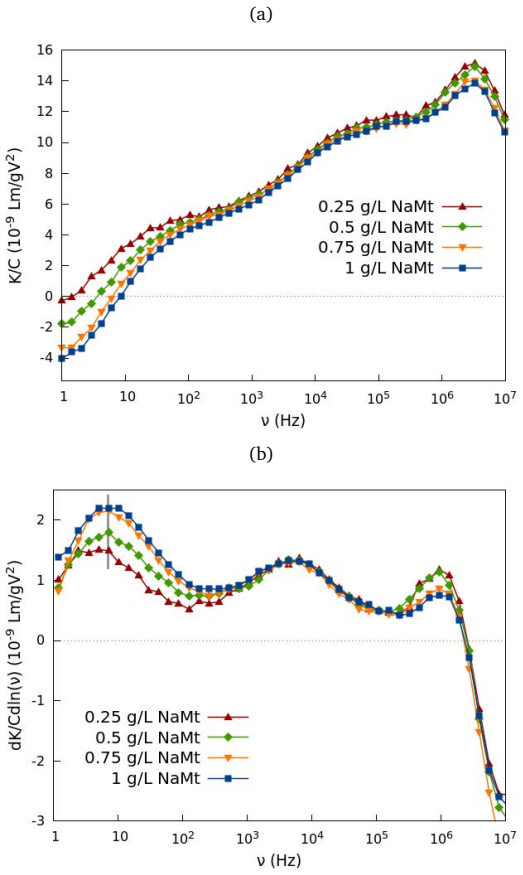

Fig. 7 a) Birefringence spectra of samples with 0.3 mM NaCl and different concentrations of NaMt. The birefringence is normalized to the particle concentration C. b) Spectrum of the logarithmic derivative of K/C. The characteristic frequency of the anomalous behaviour ($\nu_c = 7$ Hz) is indicated in grey.

(around 20 nm), particles would need to be very close for this effect to occur. Hence, some dependence of the dynamics of the system with the particle concentration would be expected, but this has not been found.

The anomalous orientation has also been observed in bidisperse systems of non spherical particles (or primary particles, PPs) and smaller (secondary) nanoparticles (SPs) of different composition.[10,15] This effect is enhanced when the SP concentration increases, whereas smaller SPs tend to produce this action for a wider frequency range. The anomalous torque experienced by the primary particles is subsequently confirmed in these cases through measurements of the turbidity of the samples for incident laser light polarized either parallel or perpendicular to the electric field.[42] The explanation for the negative K values was based on the assumption that in the low frequency range the SPs distribute themselves asymmetrically around the PPs exerting a hydrodynamic torque that forces them to orient with their minor axis along the electric field. Similarly to normal hydrodynamic torques or electrical ones, the existence of the anomalous torque should not affect the randomization time, since once the electric field is switched off, the torque dissapears and the particles disorient through a pure rotational diffusion mechanism. Also, this effect should occur at low frequency, where an asymmetric particle distribution, driven by their different electrophoretic velocities, is possible.

Such possibility is in fact theoretically confirmed in[12], where the author shows that when ions accumulate asymmetrically around a particle, they can provoke a hydrodynamic torque opposite to the electric one, producing an anomalous orientation at low enough frequencies. In the case of bidisperse systems there are not slow ions, but the mechanism described in[12] is still valid: the SPs migrate at different velocity than PPs and hence, they move asymmetrically around the particle provoking the anomalous orientation.

The anomalous effect in[15] has several similarities with our experimental results. Particularly, in our case, the role of SPs can be played by the smaller size range in the polydisperse sample, thus explaining the negative effect and the low frequency range at which it occurs. This explanation is coherent with the absence of any effect on the relaxation time, as shown in Fig. 2 and with the enhancement of the anomalous effect with the particle concentration, displayed in Fig. 7a. In contrast, the characteristic frequency at which it occurs depends only on the particles velocity, and is therefore independent of the concentration, in line with results in Fig. 7b. The pH dependence is also coherent with this picture: for acid pHs, the negatively charged faces of the smaller particles will be more strongly attracted to the positive edges of the larger ones, enhancing the anomalous orientation. In addition, increasing the ionic strength will reduce their attraction by the larger electrostatic screening. This explains the smaller significance of the anomaly for higher NaCl concentrations (Fig. 6).

5 Conclusions

The analysis described of the birefringence of sodium montmorillonite suspensions demonstrates the positive prospects of this technique and the amount of information that it can provide on such complex systems. The frequency spectra of the birefringence permits the observation of well known relaxations of the ionic clouds in EDLs, namely, α and Maxwell-Wagner. The use of classical electrokinetic theories further enables a quantitative analysis from which the surface conductivity and its anisotropy (associated to the face-edge inhomogeneous charge distribution) can be obtained. Interestingly, the low frequency range of the birefringence spectra shows anomalous negative values, that is, a tendency of the particles to orient with their faces perpendicular to the applied field, instead of parallel. Such effect is minimized at basic pHs (all surfaces are negatively charged), high ionic strengths (electrostatic screening) and low concentrations. Comparison with previous data on bimodal suspensions suggest that this behavior is the result of an additional torque induced by the interaction between the smallest particles of the size distribution of the clay and the largest ones. Such interaction necessarily occurs at low frequencies, where particle accumulation, driven by their difference velocities, is possible.

Acknowledgements

Financial support of this investigation by Junta de Andalucía, Spain (grant No. PE2012-FQM0694), MINECO, Spain (project No. FIS2013-47666-C3-1-R), Feder Funds (EU) and MINECO, Ramón y Cajal Programme (RYC-2014-16901) is gratefully acknowledged. One of the authors (P. A.) thanks MEC, Spain for her FPU grant. We also thank Professor F. Mantegazza for his help with the experimental technique.

References

1 C. T. O'Konski, *Molecular electro-optics*, Marcel Dekker, New York, 1976.

2 T. Bellini and F. Mantegazza, *Interfacial electrokinetics and electrophoresis*, Marcel Dekker, New York, 2002, pp. 401–441.

3 S. P. Stoylov and M. V. Stoivemova, *Molecular and colloidal electro-optics*, CRC Press, Boca Raton, 2006.

4 E. Frederiq and C. Houssier, *Electric dichroism and electric birefringence*, Clarendon, Oxford, 1973.

5 T. Bellini, F. Mantegazza, V. Degiorgio, R. Avallone and D. A. Saville, *Phys. Rev. Lett.*, 1999, **82**, 5160–5163.

6 M. L. Jiménez and T. Bellini, *Curr. Opin. Colloid Interface Sci.*, 2010, **15 (3)**, 131–144.

7 H. C. Benoît, *Ann. Phys.*, 1951, **6**, 561–609.

8 T. Bellini, F. Mantegazza, R. Piazza and V. Degiorgio, *Europhys. Lett.*, 1989, **10 (5)**, 499–503.

9 R. M. J. Watson and B. R. Jennings, *Powder Technol.*, 1992, **72 (1)**, 63–69.

10 M. L. Jiménez, L. Fornasari, F. Mantegazza, M. C. D. Mourad and T. Bellini, *Langmuir*, 2012, **28 (1)**, 251–258.

11 D. A. Saville, T. Bellini, V. Degiorgio and F. Mantegazza, *J. Chem. Phys.*, 2000, **113**, 6974–6983.

12 M. Fixman, *J. Chem. Phys.*, 2006, **124**, 214506.

13 V. N. Shilov, Y. B. Borkovskaja and S. N. Budankova, *Molecular and colloidal electro-optics*, CRC Press, Boca Raton, 2006, pp. 39–57.

14 R. Sasai and K. Yamaoka, *J. Phys. Chem.*, 1995, **99 (50)**, 17754–17762.

15 F. Mantegazza, M. Caggioni, M. L. Jiménez and T. Bellini, *Nat. Phys.*, 1951, **6**, 561.

16 H. Hoffmann and D. Gräbner, *Adv. Colloid Interface Sci.*, 2015, **216**, 20–35.

17 M. C. Fair and J. L. Anderson, *J. Colloid Interface Sci.*, 1989, **127 (2)**, 388–400.

18 A. V. Delgado, *Interfacial electrokinetics and electrophoresis*, Marcel Dekker, New York, 2002.

19 H. van Olphen, *An introduction to clay colloid chemistry*, Wiley, New York, 1977.

20 M. M. Ramos-Tejada, F. J. Arroyo, R. Perea and J. D. G. Durán, *J. Colloid Interface Sci.*, 2001, **235**, 251–259.

21 E. Paineau, K. Antonova, C. Baravian, I. Bihannic, P. Davidson, I. Dozov, M. Imperor-Clerc, P. Levitz, A. Madsen, F. Meneau and L. J. Michot, *J. Phys. Chem. B*, 2009, **113**, 15858–15869.

22 I. Dozov, E. Paineau, K. Antonova, C. Baravian, I. Bihannic and L. J. Michot, *J. Phys. Chem. B*, 2011, **115**, 7751–7765.

23 M. J. Shah, *J. Phys. Chem.*, 1963, **67 (10)**, 2215–2219.

24 M. J. Shah, D. C. Thompson and C. M. Hart, *J. Phys. Chem.*, 1963, **67 (6)**, 1170–17178.

25 K. Yamaoka, K. Fukudome and K. Matsuda, *J. Phys. Chem.*, 1992, **96 (17)**, 7131–7136.

26 S. Holzheu and H. Hoffmann, *J. Phys. Chem. B*, 2002, **106 (17)**, 4412–4418.

27 C. T. O'Konski, *J. Phys. Chem.*, 1960, **64**, 605–619.

28 V. N. S. S. S. Dukhin, *Dielectric phenomena and the double layer in disperse systems and polyelectrolytes*, Wiley, New York, 1974.

29 J. Lyklema, *Fundamentals of interface and colloid science, Vol II: Solid-liquid interfaces*, Academic Press, New York, 1995.

30 C. Grosse, S. Pedrosa and V. N. Shilov, *J. Colloid Interface Sci.*, 1999, **220 (1)**, 31–41.

31 R. Pecora, *Dynamic light scattering: applications of photon correlation spectroscopy*, Plenum Press, New York and London, 1985.

32 F. Mantegazza, T. Bellini, M. Buscaglia, V. Degiorgio and D. A. Saville, *J. Chem. Phys.*, 2000, **113**, 6984–6991.

33 R. Piazza, V. Degiorgio and T. Bellini, *Opt. Commun.*, 1986, **58 (6)**, 400–404.

34 H. H. Murray, *Applied clay mineralogy: occurrences, processing and applications of kaolins, bentonites, palygorskite-sepiolite, and commom clays*, Elsevier, Amsterdam, 2007.

35 C. F. Zukoski and D. A. Saville, *J. Colloid Interface Sci.*, 1986, **114 (1)**, 32–44.

36 B. R. Midmore and R. J. Hunter, *J. Colloid Interface Sci.*, 1988, **112 (2)**, 521–529.

37 A. V. Delgado, M. Cabrerizo, J. Salcedo and F. González-Caballero, *Mater. Chem. Phys.*, 1988, **20**, 232–244.

38 M. L. Jiménez, A. V. Delgado and U. Kaatze, *Annales UMCS, Chemistry*, 2008, **63**, 73–86.

39 P. B. Lorenz, *Clays and Clay Minerals*, 1969, **17**, 223–231.

40 R. W. O'Brien and W. N. Rowlands, *J. Colloid Interface Sci.*, 1993, **159**, 471–476.

41 A. Revil and P. W. J. Glover, *Geophysical Research Letters*, 1998, **25**, 691–694.

42 L. Fornasari, F. Mantegazza, M. L. Jiménez, M. Buscaglia and T. Bellini, *Phys. Rev. E*, 2009, **79**, 060401(R).